Effects of Polymer Molecular Weight on Structure and Dynamics of Colloid-Polymer Bridging Systems

Mariah J. Gallegos,* Diego D. Soetrisno,* Farshad Safi Samghabadi,* and Jacinta C. Conrad*

Department of Chemical and Biomolecular Engineering, University of Houston, Houston, 77004

E-mail: mjgalle2@central.uh.edu; ddsoetri@central.uh.edu; fsamghab@central.uh.edu; jcconrad@central.uh.edu

Abstract

We investigate the effects of polymer molecular weight on the structure and dynamics of a model colloid-polymer bridging system using confocal microscopy. Polymer-induced bridging interactions between trifluoroethyl methacrylate-co-*tert*-butyl methacrylate (TtMA) copolymer particles and poly(acrylic acid) (PAA) polymers of molecular weight $M_{\rm w}$ 130, 450, 3000, or 4000 kDa and normalized concentrations c/c^* ranging from 0.05 – 2 are driven by hydrogen bonding of PAA to one of the particle stabilizers. At a constant particle volume fraction $\phi = 0.05$, the particles form clusters or networks of maximal size at an intermediate polymer concentration and become more dispersed upon further addition of polymer. Increasing the polymer $M_{\rm w}$ at a fixed normalized concentration c/c^* increases the cluster size: suspensions with 130 kDa polymer contain small clusters that remain diffusive and those with 4000 kDa polymer form larger, dynamically arrested clusters. Biphasic suspensions with distinct populations of disperse and arrested particles form at low c/c^* , where there is insufficient polymer to bridge all particles, or high c/c^* , where some particles are sterically stabilized by the added

polymer. Thus, the microstructure and dynamics in these mixtures can be tuned through the size and concentration of the bridging polymer.

Introduction

Suspensions composed of micron-sized colloidal particles and polymers are widely used in personal care and food products, ¹ 3-D printing processes, ^{2,3} and pharmaceutical manufacturing. ⁴ The microscopic structure and hence macroscopic properties of these suspensions can be tuned by controlling the suspension composition, via the particle and polymer concentrations, and through the interactions between the particles and polymers. Non-adsorbing polymers induce interparticle depletion attractions. 5,6 Adsorbing polymers, however, can generate steric repulsions when the polymers are short, or bridging attractions if the polymers are long enough to overcome electrostatic repulsions⁷ and form bridges between two particles. 8 Further, when the surfaces of particles become fully saturated with adsorbed polymer, addition of polymer can also lead to depletion attractions. 9,10 Thus, particulate suspensions containing adsorbing polymers exhibit a rich phase behavior, including flocs and networks. Flocculation processes driven by polymers or macromolecules adsorbed to the particle surface appear in filtration applications, ^{11,12} beer fermentation, ^{13,14} and rapid diagnostics for infectious diseases. 15,16 Bridging interactions are also observed in suspensions of grafted nanoparticles or nanoemulsions, for which the solvent condition for chains, ¹⁷ grafting density, ¹⁸ bridging mechanism, ¹⁹ and polymer molecular weight ²⁰ affect the gelation and rheological behavior of the suspensions. Control over flocculation in these settings requires understanding how the interactions induced by the bridging polymers affect the microscopic properties of the suspension.

The structure of suspensions containing bridging polymers undergoes a transition from disperse particles to clusters and networks that depends on the particle and polymer concentrations as well as their relative size. Previous studies have examined the effects of polymer molecular weight on bridging suspensions on the strength of adsorption, interparticle forces, cluster size (via sedimentation or scattering measurements), and bulk rheology. In suspensions of silica particles

and poly(ethylene oxide) polymers, the strength and range of bridging interactions depended on the surface coverage (which determines the conformation of adsorbed polymer), such that the state behavior depended on the relative size of particles and polymers as well as polymer concentration and molecular weight. 8 In kaolin-polyethyleneimine suspensions, increasing the polymer concentration reduced the density and increased the fractal dimension of clusters; increasing the polymer molecular weight promoted bridging interactions between particles and polymers but did not strongly affect the yield stress. ²¹ In kaolin-polyacrylamide suspensions, an increase in the polymer molecular weight slightly increased the cluster size and reduced the fractal dimension of flocs. ²² In polystrene-polydiallyldimethyl ammonium suspensions, increasing the polymer molecular weight led to greater surface coverage by the bridging polymers. ²³ In suspensions of silica particles and poly(ethyleneimine) polymers, the yield stress was greatest for the highest polymer molecular weight. ²⁴ Suspensions of silica particles and poly(acrylic acid) polymers exhibited shear thickening when the polymer molecular weight was sufficiently high to allow particles to be bridged by flexible coils; intriguingly, the suspensions with the highest polymer molecular weight ($M_{\rm w} = 7.5 \times 10^5$ g mol⁻¹) did not shear-thicken, because the long adsorbed polymers desorb before they are fully extended by the flow. 25 In suspensions of silica particles and poly(ethyleneimine) polymers, the greatest yield stress was observed for the largest polymer ($M_{\rm w} = 70,000~{\rm g~mol^{-1}}$). ²⁴ Most experiments, therefore, have focused on the effects of the particle-polymer size ratio on macroscopic (flow) properties. How the polymer size affects the microscopic structure and dynamics remains incompletely understood.

Confocal microscopy experiments allow particles to be visualized at the microscopic scale and thus provide an intriguing option for investigating the microscopic structure and dynamics of bridging suspensions. Only a few studies, however, have applied this method to investigate the behavior of suspensions with polymer-mediated bridging interactions. Confocal imaging on suspensions of clay, bitumen, and an anionic polymer flocculant revealed qualitative changes in the density and packing of flocs with increasing polymer concentration. ²⁶ Single-particle tracking experiments on silica-polyethylene suspensions showed that the microstructure and dynamics of these suspensions

varied strongly with particle and polymer concentration: below a critical polymer concentration at which the maximum storage modulus was observed, suspensions contained both mobile (disperse) and arrested (aggregated) particles.²⁷ How polymer molecular weight affects the microscopic properties of bridging suspensions has not been explored, to our knowledge, and is the focus of this study.

Using fluorescence confocal microscopy, we show that the polymer molecular weight affects the microscopic structure and dynamics of colloid-polymer bridging systems. We synthesized coreshell copolymer particles that were sterically and electrostatically stabilized through grafted polymers on the particle surface and that could be refractive index- and density-matched to 80(w/w)% glycerol-water. ^{28,29} Bridging interactions are induced by the addition of poly(acrylic acid) (PAA), which forms hydrogen bonds with the steric and electrostatic polymer brush stabilizers. In our previous study, we showed that the structure and dynamics of these suspensions could be tuned through the pH-dependent bridging interactions. ³⁰ In this study, we characterized the microscopic structure and dynamics of suspensions at a constant particle volume fraction $\phi = 0.05$ containing PAA of various molecular weights (130, 450, 3000, and 4000 kDa) at normalized polymer concentrations c/c^* (where c^* is the polymer overlap concentration) ranging from 0.05 to 2. For all four $M_{\rm w}$, metrics for particle structure and dynamics exhibit non-monotonic trends as a function of c/c^* , consistent with a growing fraction of sterically-stabilized polymers above a threshold concentration. Increasing the molecular weight of PAA at a fixed c/c^* generally leads to the formation of larger clusters, likely due to the larger polymer radius of gyration. Finally, distinct populations of free and aggregated particles are obtained at $c/c^* = 0.05$ for all four polymers and at high c/c^* for the two highest molecular weight polymers. Thus, the polymer $M_{\rm w}$ provides additional control over the structure and dynamics of polymer-bridged colloidal suspensions.

Materials and Methods

Copolymer particle synthesis

All chemicals for particle synthesis were purchased from Sigma Aldrich unless specified otherwise. Poly(2,2,2-trifluoroethyl methacrylate-co-tert-butyl methacrylate) (TtMA) particles were synthesized using previously reported procedures. ^{28,29} Briefly, we first synthesized fluorescent particle cores, then grew a non-fluorescent shell, and finally grew charged stabilizer polymers on the particle surface using atom transfer radical polymerization (ATRP). A volumetric ratio of 45:55 of 2,2,2trifluoroethyl methacrylate (TFEMA; SynQuest Lab) to tert-butyl methacrylate (tBMA) was used to obtain TtMA copolymer particles of diameter 1.63 \pm 0.03 μ m that were density- and refractive index-matched to 80 (w/w)% glycerol-water. Rhodamine B methacrylate was incorporated during core synthesis for confocal imaging. 2-(2-bromoisobutyryloxy)ethyl acrylate (initator monomer) was added during core and shell synthesis as a growth initiator for addition of charged polymer on the copolymer particle surface. In that final synthesis step, a negatively charged copolymer composed of 2-acrylamido-methyl-1-propanesulfonic acid and dimethylacrylamide was grown on the copolymer particle surface via ATRP³¹ using a 1:1 input ratio of methanol:water. The charged copolymer particles were collected and washed using Millipore water and centrifuged five times at 2000 rpm for 5 minutes to remove any unreacted reagents. After the final centrifugation, glycerol was added to the particle pellet to obtain a stock of $\phi \sim 0.46$ in 60 (w/w)% glycerol-water. The particle stock was centrifuged for 2.5 hours, after which glycerol was added to obtain a particle volume fraction of $\phi \sim 0.49$ in 80 (w/w)% glycerol-water. The stock was mixed once more then centrifuged at 2000 g for 3 minutes to remove bubbles that appeared during mixing. The glass vial containing the particle stock was sealed with Parafilm and stored in an explosive-proof refrigerator.

Particle characterization

The hydrodynamic diameter d_h of the TtMA copolymer particles in water was measured using dynamic light scattering (DLS) on a 3-D LS Spectrometer (LS Instruments; Switzerland). Five

correlation functions per angle were collected for 60 seconds at scattering angles of 30, 60, 90, 120, and 150 degrees. The internal temperature was held constant at 25°C. The correlation functions were fitted using a single exponential decay cumulant,

$$g^{(2)}(\tau, q) - 1 = \beta \exp(-2\Gamma \tau) \left(1 + \frac{\mu_2}{2} \tau^2 \right)$$
 (1)

where $\beta \approx 1$ is a correction factor that depends on the instrumental scattering geometry, $\Gamma(q)$ is the average decay rate, $\tau(q)$ is the exponential decay time, μ_2 is the second moment of the distribution, and q is the scattering vector ($q = \frac{4\pi n}{\lambda} \sin(\theta/2)$). For q, n = 1.333 is the refractive index of water, λ is the laser wavelength (660 nm), and θ is the scattering angle. We calculated the diffusion coefficient D via $\Gamma = Dq^2$ and subsequently calculated the hydrodynamic diameter using the Stokes-Einstein equation, $d_H = k_B T/3D\pi\eta$, where k_B is the Boltzmann constant, T is temperature, and η is the solution viscosity. We report d_H with a 95% confidence interval.

The zeta potential ζ of the charged copolymer particles was measured using a Nicomp 380 ZLS zeta sizer. For a suspension of TtMA particles at $\phi = 0.001$ in a 10 mM Trizma buffer solution at pH 7.5, $\zeta = -76 \pm 2$ mV, consistent with literature values. ^{28–30}

PAA stock preparation

Poly(acrylic acid) (PAA) powders of four molecular weights (130, 450, 3000, and 4000 kDa) were purchased from Sigma Aldrich. Glass dram vials were cleaned three times with toluene and left to dry overnight in a fume hood. Dried vials were washed five times with Millipore water then placed into an oven at 100°C for 3 hours. To create a PAA stock solution at a given molecular weight, PAA powder was weighed and poured into the clean glass vials. Millipore water was added to vials, which were sealed with Parafilm and then placed onto a horizontal mixer. (We add extra glycerol during suspension preparation to obtain a final solution concentration of 80(w/w)% glycerol-water.) The polymer stock solutions were mixed for at least a week for low molecular weights (130 and 400 kDa) and up to two weeks for high molecular weights (3000 and 4000 kDa). After polymer stock

solutions were completely homogenized, vials were taken off the roller and stored in a desiccator.

PAA contour length

The contour length of PAA was calculated for both a fully extended linear chain $(L_{v,l})$ and tetrahedral configuration $(L_{v,t})$. Contour length is based on polymer chain geometry, which does not depend on solvent. The linear contour length is defined as $L_{v,l} = N_v L_0$ and the tetrahedral configuration contour length is defined as $L_{v,t} = N_v L_0 sin(\theta/2)$ where N_v is the viscosity-average degree of polymerization, L_0 is the length of one carbon-carbon bond, and $\theta = 109.5^{\circ}$ is the carbon-carbon bond angle. Values of $L_{v,l}$ and $L_{v,t}$ are reported in Table 1 for all PAA molecular weights. PAA is not expected to be in the fully extended configuration as it may absorb at multiple points along its backbone. ²⁵

Sample preparation

Stock suspensions of TtMA copolymer particles in glycerol-water and aqueous solutions of PAA were combined to produce colloidal-polymer suspensions at volume fractions $\phi = 0.01$ and 0.15 at normalized polymer concentrations of $c/c^* = 0.05$, 0.1, 0.3, 0.5, 0.7, 1, and 2. To account for the missing glycerol in the PAA stock, additional glycerol was added to ensure that the solvent composition was 80(w/w)% glycerol-water. Suspensions were tumbled for three to five days to ensure that they were homogenized. Once completely mixed, vials were centrifuged for three minutes at 200 g to remove any bubbles before imaging.

We constructed glass chambers for imaging experiments using glass cover slides and UV-curable epoxy (Norland Optical). A microscope glass slide (VWR) was cut into two roughly 20 mm \times 15 mm pieces. These pieces were glued onto a 48 mm \times 65 mm \times 0.15 mm glass cover slip (VWR). To create a chamber, we added a third cover slip (VWR) of dimensions roughly 25 mm \times 25 mm \times 0.2 to the top of the glass slide pieces. Approximately 100 μ L of suspension was pipetted into the glass chamber, which was sealed using UV-curable epoxy. We imaged enclosed suspensions roughly 30 minutes after removal from the horizontal roller.

Confocal imaging and tracking analysis

A Leica DMi8 fluorescence microscope with confocal headseries Leica SP8 equipped with a 63x oil-immersion objective was used to image the suspensions. To characterize the 3-D structure of the particles, series of 3-D images were captured at vertical positions from 25 to 65 μ m at a step size of 0.1 μ m. Ten of these image series were acquired at 13.8 frames per second (fps) at different spatial locations within the chamber. To characterize the particle dynamics, 2-D images were collected as a function of time at a fixed position of 30 μ m above the bottom of the coverslip and a frame rate of 9.4 fps for 1000 frames. Ten of these 2-D image series were collected at different locations within the suspension. For 2-D images, a tracking algorithm was used to link the particle centroids into trajectories over time. ³² We report a static 2-D tracking error of \pm 39 nm determined from a dilute particle suspension in the absence of polymer to ensure particles are fully diffusive. For 3-D images, the z-positions of the particle centroids were located to submicron accuracy. ³³

From the 3-D particle trajectories, we calculate the radial distribution function g(r), contact number (CN), and number density fluctuation NDF = $\frac{\langle N^2 \rangle - \langle N \rangle^2}{\langle N \rangle}$, where N is the number of particles in a defined cubic box of length L. From the 2-D particle trajectories, we calculate the ensemble-averaged mean-square displacement MSD = $\langle (x(t+\tau)-x(t))^2 \rangle$, self part of the van Hove correlation function $G(x,t) = \frac{1}{N} \sum_{n=1}^{\infty} \delta(x - [x_i(t) - x_i(0)])$, and radius of gyration R_g of particle trajectories.

Results and Discussion

Particle aggregation depends on polymer size

We previously investigated the effects of pH and PAA polymer concentration on the polymer-bridging-driven aggregation of TtMA particles using confocal microscopy.³⁰ The attractive bridging interaction between the particles is driven by hydrogen bonding between PAA and one or both grafted polymers on the surface of the TtMA particles.^{34,35} In this study, we fixed the concen-

tration of the particles ($\phi = 0.05$) and examined the effects of molecular weight $M_{\rm w}$ on the suspension structure and dynamics. The polymer radius of gyration $R_{\rm g}^p$, linear configuration contour length $L_{v,l}$, and tetrahedral configuration contour length $L_{v,l}$ of PAA increase with increasing $M_{\rm w}$ (Table 1). Polymer radius of gyration was calculated from intrinsic viscosity using the two-term virial expansion of viscosity, $\eta = \eta_0(1 + [\eta]C_{PAA})$, where $[\eta]$ is the intrinsic viscosity, η_0 is the solvent viscosity, and C_{PAA} is the polymer concentration, for all PAA molecular weights in 80(w/w)% glycerol-water. ³⁶ Prior work showed that the conformation of the adsorbed polymer depends on the surface coverage and molecular weight, which in turn affects the strength and range of the bridging interactions. ⁸ Because longer polymers are more likely to be able to extend beyond the range of electrostatic repulsion of the particles, we expect that changing the polymer molecular weight will affect the structure and dynamics of the TtMA suspensions. Based on prior studies, ⁸ we expect that larger flocs will form as the molecular weight of the polymer is increased. The increase in floc size manifested in both the volume and number of particles in a floc (illustrated schematically in Figure 1(a) - (d)).

Table 1: PAA properties: viscosity average molecular weight M_v , polymer radius of gyration R_g^p , size ratio R_g^p/a (using particle radius a=815 nm), overlap concentration c^* , linear configuration contour length $L_{v,l}$, and tetrahedral configuration contour length $L_{v,l}$.

M_v (kDa)	R_g^p (nm)	$R_g^p/a~(\times 10^{-2})$	$c^* \text{ (mg mL}^{-1})$	$L_{v,l}$ (nm)	$L_{v,t}$ (nm)
130	26.3	3.23	2.3	278	227
450	30.4	3.73	5.7	962	785
3000	56.7	6.95	6.5	6411	5236
4000	67.4	8.27	5.2	8548	6981

At a constant normalized polymer concentration of $c/c^* = 0.3$, the polymer molecular weight indeed alters the structure of aggregates. Particles bridged by the largest polymers (4000 kDa, Figure 1(h)) form larger flocs than those bridged by the smallest polymers (130 kDa, Figure 1(e)). The polymer size also affects the number of free particles. Suspensions containing $M_w = 130$ kDa polymers contain free particles as well as small clusters, whereas nearly all particles belong to clusters in suspensions containing $M_w = 4000$ kDa polymers. This observation is also consistent

with the idea that larger polymers can more readily overcome the electrostatic repulsions between particles. Representative confocal micrographs for the other normalized polymer concentrations are shown in Supplementary Information (Figure S1).

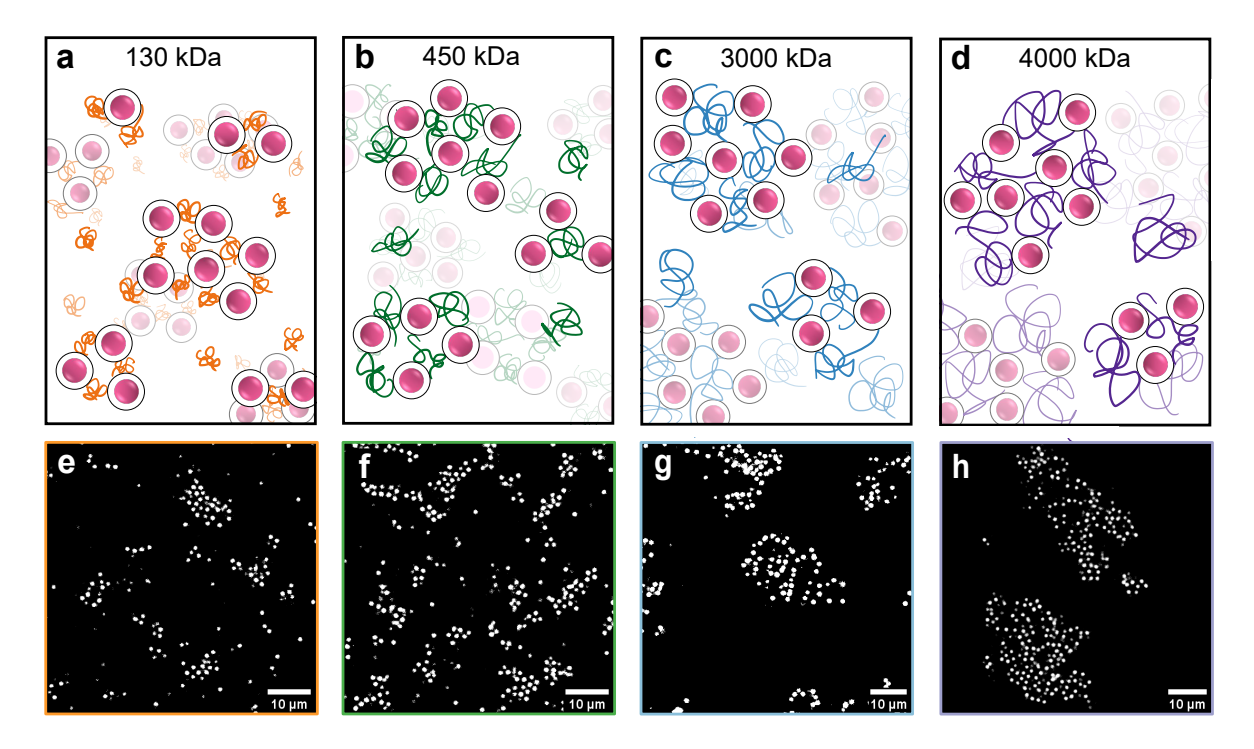


Figure 1: (a-d) Schematic representation (not to scale) of bridging of TtMA particles (pink) by PAA polymers of molecular weight 130 (a; orange), 450 (b; green), 3000 (c; blue), and 4000 kDa (d; purple). (e-h) Static confocal micrographs of bridging suspensions $\phi = 0.05$ containing PAA of molecular weight 130 (e), 450 (f), 3000 (g), 4000 kDa (h) at a constant normalized polymer concentration $c/c^* = 0.3$. The brightness and contrast of each micrograph have been adjusted for clarity. The scale bars indicate 10 μ m.

Structure of suspensions with 130 and 4000 kDa PAA

We first examined the effects of PAA $M_{\rm w}$ on the structure of TtMA bridging suspensions for normalized polymer concentrations c/c^* ranging from 0.05 to 2. We present the characterizations of the lowest (130 kDa) and highest (4000 kDa) molecular weights; data for the intermediate $M_{\rm w}$ values are presented in the SI (Figure S2)). For suspensions containing a low- $M_{\rm w}$ polymer (130 kDa), the radial distribution function g(r) exhibits a sharp local maximum at interparticle contact $(r/2a \approx 1)$ and a second local maximum at $r/2a \approx 1.8$ (Figure 2(a)). The presence of first- and

second-neighbor shells are consistent with previous structural measurements on arrested colloidal depletion gels.³⁷ The height of the first maximum increases concomitant with PAA concentration up until $c/c^* = 0.3$. At higher polymer concentrations, the height of the first maximum decreases with addition of PAA, consistent with the decrease in clustering observed in our previous study at high concentrations of PAA.³⁰ At the highest concentrations of PAA examined($c/c^* = 1-2$), g(r) approximates a step function with only a weak local maximum. This result is consistent with saturation of the particle surfaces with the polymer, such that the polymer acts as a steric stabilizer to generate repulsive interactions.^{38,39}

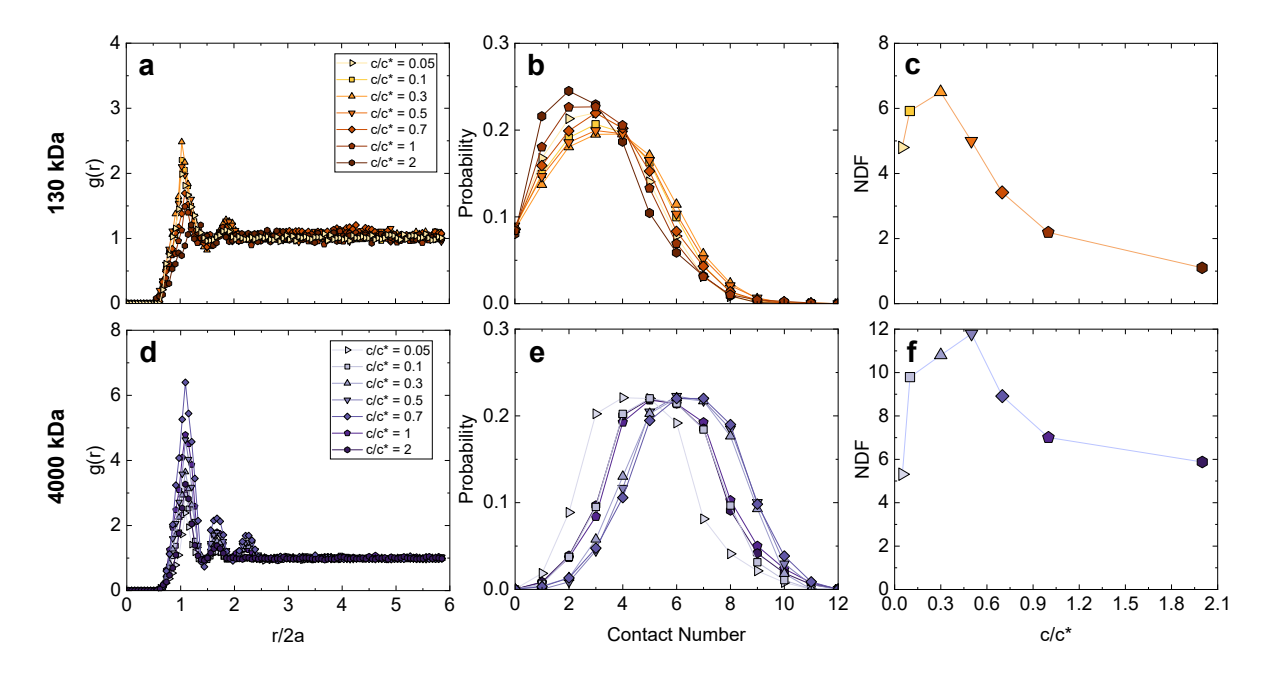


Figure 2: (a,d) Radial distribution function g(r) as a function of normalized distance from the particle r/2a for PAA molecular weight of (a) 130 and (d) 4000 kDa. (b,e) Probability distribution of contact number for PAA molecular weight of (b) 130 and (e) 4000 kDa. (c,f) Number density fluctuation (NDF) as a function of normalized polymer concentration c/c^* for PAA molecular weight of (c) 130 and (f) 4000 kDa. The particle volume fraction is $\phi = 0.05$ in all suspensions. Symbols indicate the normalized polymer concentration: $c/c^* = 0.05$ (\triangleright), 0.1 (\blacksquare), 0.5 (\triangleright), 0.5 (\triangleright), 1 (\spadesuit), and 2 (\spadesuit).

As a second measure for short-range structure, we calculated the contact number (CN) distribution, using a distance cutoff of r/2a = 1.6 that was determined from the first minimum in g(r) of the most flocculated suspension (i.e., the suspension that contains the largest clusters) $(c/c^* = 0.3)$. Increasing c/c^* leads to pronounced changes in the distributions of CN. For suspensions

containing 130 kDa polymer with c/c^* of 0.05 to 0.3, the CN distribution exhibits a maximum at \approx 4, indicating that the most likely number of nearest neighbors is 4 (Figure 2(b)). The probability of CN > 4 increases as c/c^* approaches 0.3. As normalized polymer concentration is increased further $(c/c^* > 0.3)$, the peak in the CN distributions shifts to lower CN \approx 2. At $c/c^* = 2$, the maximum is located at CN \approx 2, consistent with a suspension that contains both dispersed particles and small clusters. The evolution in the CN distribution with increasing c/c^* for low normalized polymer concentrations is consistent with measurements on a silica-PEI ($\phi = 0.30$, $M_n = 1200$) bridging gel, for which the increase in CN was attributed to the increasing number of particles belonging to the arrested network. ²⁷ At the higher volume fraction, Ref. 27 did not observe non-monotonic changes in the microscopic properties with polymer concentration, although the mechanical properties (i.e., elastic modulus) exhibited a local maximum at an intermediate concentration. In our system, however, the non-monotonic dependence of the CN maximum on c/c^* likely reflects the steric stabilization (i.e., increasing dispersion) of the particles. Full steric stabilization occurs at $c/c^* \approx 1.7$ for this M_w (Figure S10(a)); thus, we posit that the decrease in CN above $c/c^* = 0.5$ reflects the stabilization of an increasing fraction of particles.

To quantify the cluster structure on longer length scales, we calculate the number density fluctuations (NDF) at a normalized length scale of a/L=0.16, in which $L=5\mu m$ is the binsize (Figure 2(c)). We select the length scale a/L as the location of the maximum in NDF(L) of the strongest gel ($c/c^*=0.3$) at this $M_{\rm w}$, following established protocols. 30,37 The NDF ≈ 5 at $c/c^*=0.05$ and increases to ≈ 7 for $c/c^*=0.3$, consistent with the formation of clusters of particles (i.e., increasing spatial heterogeneity). As c/c^* is increased beyond 0.3, however, the NDF decreases and approaches ≈ 1 at the highest normalized polymer concentration ($c/c^*\approx 2$), indicating that the particle structure becomes more uniform on this length scale. In this system, the decreases in the most-probable CN combined with the decrease in the NDF suggests that the particles are increasingly dispersed at higher c/c^* . This result is in contrast to the decrease in NDF with increasing polymer concentration observed for the higher- ϕ gels in Ref. 27, which reflected the increasingly uniform structure of an arrested, elastic gel network.

Increasing the molecular weight of the polymer to 4000 kDa alters the trends in the evolution of structure with increasing polymer concentration. All suspensions containing the 4000 kDa polymer exhibit a pronounced first local maximum in g(r) (Figure 2(d)). The height of the first maximum increases with polymer concentration up to $c/c^* \approx 0.7$, a higher concentration than for the 130 kDa polymers, and subsequently decreases. At a given c/c^* , the height of this first local maximum is greater than that of the corresponding 130 kDa sample, indicating that the particles exhibit stronger local structural correlations in the presence of the higher- $M_{\rm w}$ polymer. The g(r) for the 4000 kDa samples exhibit both second- and third-local maxima at all concentrations, suggesting that larger clusters 37 form in the presence of a higher- $M_{\rm w}$ bridging polymer. As normalized polymer concentration is increased above $c/c^* = 0.7$, the heights of all three maxima decrease, indicating that the nearest-neighbor correlations weaken at high normalized polymer concentrations.

The contact number distributions for suspensions containing 4000 kDa polymers exhibit local maxima at higher CN values (at comparable c/c^*) than those at corresponding c/c^* values for the 130 kDa polymers (Figure 2(e)). The value of CN at the maximum is, again, a non-monotonic function of the normalized polymer concentration, increasing from ≈ 4 at $c/c^* = 0.05$ to $\approx 6 - 7$ at $c/c^* = 0.7$, and then decreasing to $\approx 5 - 6$ at $c/c^* = 2$. The greater CN at the local maximum is consistent with the strong interparticle correlations inferred from g(r), and with the order-of-magnitude greater number of binding sites on this polymer compared to the 130 kDa polymer (SI Table S1). Likewise, the decrease in CN at higher normalized polymer concentrations is consistent with the decrease in the maxima of g(r). The steric stabilization concentration for this sample is $c/c^* = 4.8$ (Figure S10(b)), and we posit that the decrease in CN above $c/c^* = 0.7$ again reflects an increasing fraction of disperse, sterically-stabilized particles.

Finally, we examined the NDF for the 4000 kDa polymer using a/L = 0.13 (corresponding to $L = 6 \ \mu m$, the location of the maximum in NDF(L) for the strongest gel; Figure 2(f)). The NDF increased from ≈ 5 at $c/c^* = 0.05$ to a local maximum of ≈ 12 at $c/c^* = 0.7$, then decreased to ≈ 6 as c/c^* approached 2. Suspensions containing 4000 kDa polymers exhibited stronger number density fluctuations (i.e., greater NDF at equal c/c^*) compared to those containing 130 kDa polymers,

consistent with the formation of larger clusters. This result is qualitatively consistent with the observation of larger flocs in the kaolin-polyacrylamide bridging suspensions of Ref. 22.

Dynamics of suspensions with 130 and 4000 kDa PAA

We first characterize the mean-square displacements (MSDs) of TtMA particles in bridging suspensions containing 130 and 4000 kDa PAA (data for the other two molecular weights are shown in Figure S3 in the SI.) We report the MSDs in absolute time, noting that the viscosities of charged polymer solutions of various $M_{\rm w}$ at the same c/c^* are equal; ⁴⁰ MSDs corrected for the change in the background viscosity due to the presence of the polymer are shown in SI (Figure S8). For suspensions containing 130 kDa polymers, the MSDs are subdiffusive (i.e., exhibit a logarithmic slope of less than 1) on short time scales and exhibit approximately diffusive scaling (i.e., exhibit a logarithmic slope close to 1) on long time scales (Figure 3(a)). The magnitudes of the MSDs on long time scales exhibit weak re-entrance as a function of normalized polymer concentration, first decreasing as c/c^* is increased up to 0.05 and then increasing at higher normalized polymer concentrations such that the fastest diffusion (i.e., greatest MSD) occurs at $c/c^* = 2$. This trend is consistent with the re-entrant changes in structure as a function of c/c^* (Figure 3) and thus likely reflect the formation of larger and then smaller clusters with increasing normalized polymer concentration as the surfaces of the particles become saturated by the polymers. ¹⁰

On short time scales ($\tau=0.5$ s), the shape of the self part of the van Hove correlation function $G(\Delta x,\tau)$ depends on the polymer concentration. For suspensions with $c/c^*=0.05$, $G(\Delta x,\tau)$ is non-Gaussian and exhibits pronounced extended tails (Figure 3(b)). The width of $G(\Delta x,\tau)$ increases with normalized polymer concentration up to $c/c^*=0.5$, but the distributions are less non-Gaussian. Upon further increasing the polymer concentration, the width of the distribution decreases and $G(\Delta x,\tau)$ becomes approximately Gaussian at $c/c^*=2$. Qualitatively similar non-monotonic dependence of $G(\Delta x,\tau)$ on c/c^* is observed at a longer lag time $\tau=5$ s (Figure 3(c)). For this τ , however, the width of the distribution is greatest at $c/c^*=0.3$ and decreases with increasing normalized polymer concentration thereafter, with the distribution at $c/c^*=2$ again approxi-

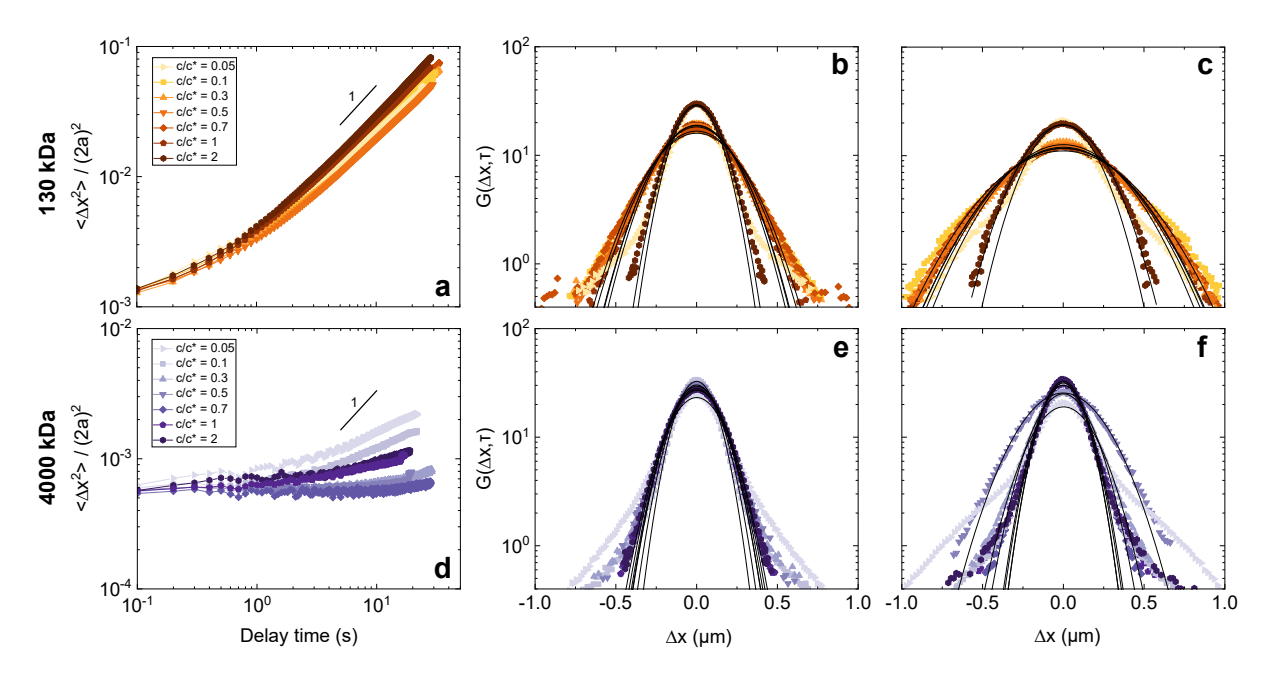


Figure 3: (a,d) Normalized MSD $\langle \Delta x^2 \rangle / (2a)^2$ as a function of delay time τ for PAA molecular weight of (a) 130 and (d) 4000 kDa. (b,c,e,f) van Hove correlation functions $G(\Delta x, \tau)$ as a function of displacement Δx at lag times τ of (b,e) 0.5 seconds and (c, f) 5 seconds. The particle volume fraction is $\phi = 0.05$ in all suspensions. Symbols indicate the normalized polymer concentration: $c/c^* = 0.05$ (\triangleright), 0.1 (\blacksquare), 0.3 (\triangle), 0.5 (\blacktriangledown), 0.5 (\spadesuit), 1 (\spadesuit), and 2 (\spadesuit). Gaussian fits to each of the van Hove plots (b,c,e,f) are shown in black.

mating a Gaussian. Given that these samples are not dynamically arrested, the strikingly extended tails in the low c/c^* samples likely exhibit distinct populations of mobile and arrested particles.²⁷

By contrast, the particle dynamics in suspensions containing a higher molecular weight PAA, $M_w = 4000 \text{ kDa}$, are nearly arrested at all polymer concentrations. For all c/c^* , the slope of the MSD is nearly zero, consistent with dynamic arrest and hence gel-like behavior on accessible time scales (Figure 3(d)). The observed near-arrest is consistent with the large flocs observed for suspensions with $M_w = 4000 \text{ kDa}$ (Figure 2(d-f)), whose formation is driven by the larger R_g^p of this polymer. On longer time scales, the MSDs for all samples increase slightly, and exhibit a non-monotonic dependence on polymer concentration (as also observed for the 130 kDa samples). The magnitude of the MSD first decreases as c/c^* is increased to 0.7, and subsequently increases upon further addition of polymer up to $c/c^* = 2$. The weakly non-monotonic dependence of the MSD is consistent with the trend in changes in structure with increasing polymer concentration (Figure 2(d-f)).

For suspensions containing 4000 kDa PAA, the evolution of the van Hove correlation function $G(\Delta x, \tau)$ with polymer concentration exhibits qualitatively different trends than for the smaller polymer. As for the smaller 130 kDa PAA, $G(\Delta x, \tau)$ has extended tails at $c/c^* = 0.05$ for both $\tau = 0.05$ s (Figure 3(e)) and 5 s (Figure 3(f)). The width of the distribution, however, decreases monotonically (save for $c/c^* = 0.5$ at $\tau = 5$ s) as c/c^* is increased. Similarly extended tails have been observed in bridging 27 as well as depletion 37 gels, and in dynamically arrested systems are typically attributed to heterogeneous dynamics. Confocal micrographs of this sample (Figure S1), however, show disperse as well as flocculated particles, suggesting that these extended tails may have a different origin than in fully-aggregated suspensions.

Biphasic behavior at low c/c^*

The differences in the width and shape of the van Hove distributions with concentration (Figure 3) and the sample micrographs (Figure S1) suggest that the dynamics may include contributions from distinct populations of particles²⁷ at selected values of c/c^* and $M_{\rm w}$. To identify such biphasic

dynamics in our suspensions, we applied a criterion from Ref. 27 and examined the dependence of the trajectory radius of gyration R_g on the number of points in the trajectory N. We observe three different types of sample dynamics across the range of polymer $M_{\rm w}$ and c/c^* examined. First, suspensions with 4000 kDa PAA at a concentration of $c/c^* = 0.05$ contain two populations of particles: a diffusive population, for which R_g increases with N, and an arrested population, for which R_g is approximately independent of N (Figure 4(a)). The diffusive and arrested populations respectively fall above and below the straight line in Figure 4(a). We do not observe exchange of particles between clusters and the dispersed phase, likely due to the strength of the multivalent hydrogen bonds between the polymer and the particle stabilizer. The observation of biphasic dynamics in this sample is consistent with the confocal micrographs, which reveal both free and flocculated particles (SI Figure S1). Suspensions with 4000 kDa PAA at a concentration of $c/c^* = 0.5$, however, contain only one population of arrested particles (Figure 4(b)), whereas suspensions with 130 kDa PAA at a concentration of $c/c^* = 2$ contain only one population of diffusive particles (for which R_g increases with N, Figure 4(c)). Notably, biphasic behavior occurs where distinct populations of disperse and arrested particles form at low c/c^* (for all $M_{\rm w}$), where there is insufficient polymer to bridge all particles, or high c/c^* (for 4000 kDa), where the suspensions contain some sterically stabilized particles alongside particles in clusters. Both observations are consistent with expectations based on confocal microscopy (SI Figure S1).

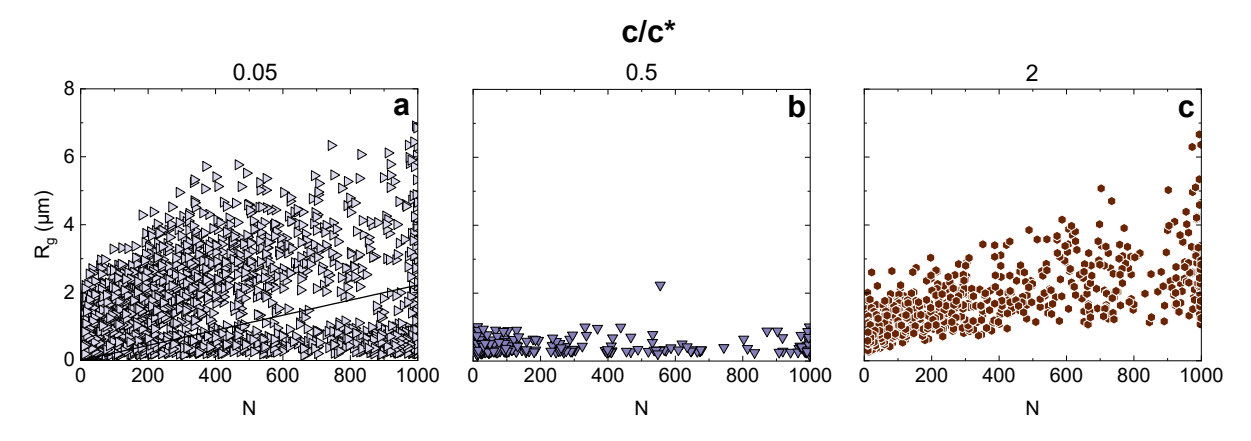


Figure 4: (a-c) Radius of gyration of particle trajectories R_g as a function of the number of points in the trajectory N for suspensions containing PAA of M_w (a) 4000 kDa at $c/c^* = 0.05$, (b) 4000 kDa at $c/c^* = 0.5$, and (c) 130 kDa at $c/c^* = 2$. The black line in (a) separates the diffusive (above) and arrested (below) populations.

Using the dependence of R_g on N to identify and distinguish diffusive and arrested particles, we examine the connection between the dynamics and structure of the 130 and 4000 kDa suspensions as a function of c/c^* (Figure 5). Two types of trajectories are observed for suspensions with 130 kDa and $c/c^* = 0.05$ and 0.5: diffusive (Figure 5(a,d)) and arrested (Figure 5(b,e)). 3-D renderings of these samples, meanwhile, also reveal distinct populations of particles with high (clustered) and low (disperse) CN values (Figure 5(c,f)). These samples thus exhibit biphasic behavior, with distinct populations of disperse and flocculated particles. Increasing the normalized polymer concentration from $c/c^* = 0.05$ to 0.5 drives a decrease in the population of disperse particles and a concomitant increase in flocculation (i.e., in particles with higher CN). At $c/c^* = 2$, however, the trajectories are approximately diffusive and particles are largely disperse (Figure 5(i)). These results suggest that the particles are fully stabilized by 130 kDa polymer at high concentrations.

Biphasic behavior is less pronounced upon increasing the polymer $M_{\rm w}$ to 4000 kDa, consistent with the enhanced flocculation observed in these samples. Suspensions with $c/c^*=0.05$ exhibit biphasic behavior, as indicated by two types of trajectories and by the observation of flocculated and disperse particles in 3-D renderings reconstructed from z-stack particle positions (Figure 5(j-1)). Increasing the normalized polymer concentration to $c/c^*=0.5$ drives the formation of large clusters in which all particles have many nearest neighbors, and particles primarily exhibit arrested

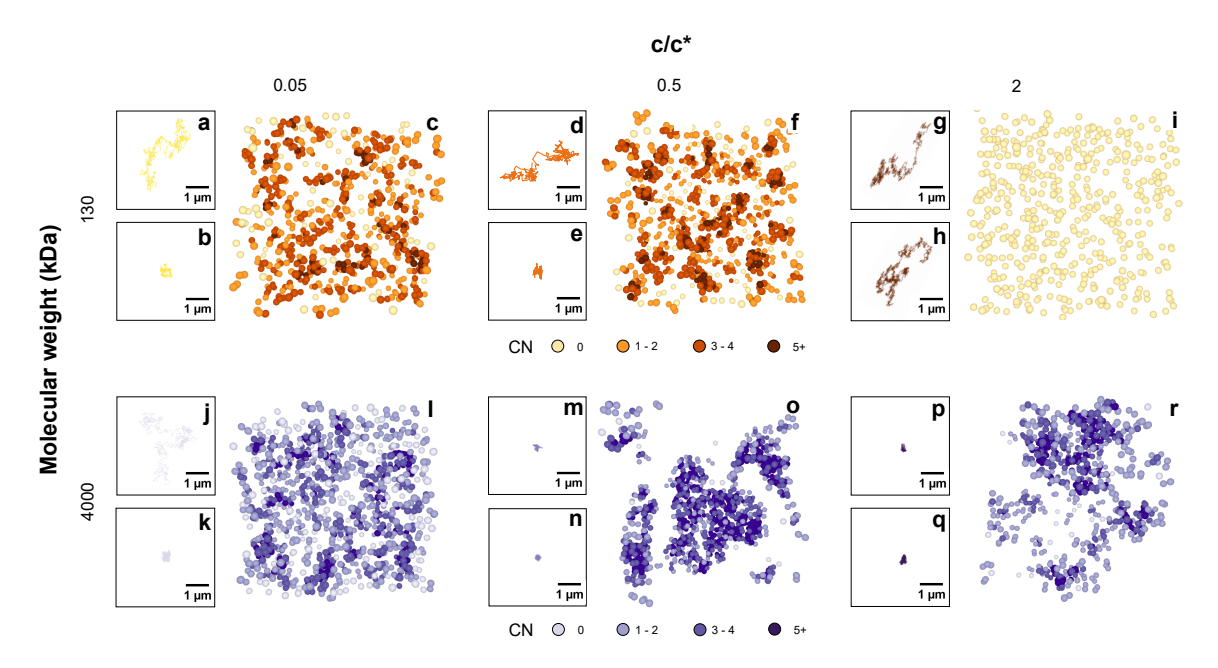


Figure 5: Representative particle trajectories of (a,d,g,h,j) a freely diffusing particle and (b,e,k,m,n,p,q) an arrested particle for PAA molecular weight of (a,b,d,e,g,h) 130 and (j,k,m,n,p,q) 4000 kDa at $c/c^* = 0.05$ (a,b,j,k), 0.5 (d,e,m,n), and 2 (g,h,p,q). (c,f,i,l,o,r) 3-D renderings (thickness $\Delta z \approx 13 \ \mu m$) of suspensions with $\phi = 0.05$ and $c/c^* = 0.05$ (c,l), 0.5 (f,o), and 2 (i,r) for PAA $M_{\rm w}$ 130 (c,f,i) and 4000 kDa (l,o,r). Particle color indicates its contact number (CN).

trajectories (Figure 5(m-o)). Finally, suspensions with $c/c^* = 2$ form looser clusters, as indicated by the slightly lower CN values compared to $c/c^* = 0.5$, and the particle trajectories are mostly arrested (Figure 5(p-r)). Thus, the polymer size affects the propensity of suspensions to form biphasic mixtures.

State diagram for bridging suspensions

We summarize the data on bridging suspensions formulated with polymers of different $M_{\rm w}$ and c/c^* on a state diagram. As a metric, we examine the NDF as a function of the c/c^* and $M_{\rm w}$ (Figure 6). For each polymer $M_{\rm w}$, the NDF first increases and then decreases as a function of normalized polymer concentration. The range of NDF values and the value of c/c^* at which the NDF attains its maximum are distinct for the low (130, 450 kDa) and high (3000, 4000 kDa) $M_{\rm w}$ polymers. For suspensions containing 130 and 450 kDa polymers, the NDF values range from ≈ 1 to ≈ 9 , and the maximum NDF occurs at $c/c^* \approx 0.3$. For suspensions containing 3000 and 4000 kDa polymers,

the NDF values range from ≈ 5 to ≈ 12 , indicating that larger polymers lead to suspensions with greater structural heterogeneity. Further, the maximum NDF for these suspensions occurs at a slightly higher value, $c/c^* \approx 0.5$. At a constant c/c^* (i.e., approximately constant background viscosity), the structures become more heterogeneous (larger NDF) as the $M_{\rm w}$ is increased.

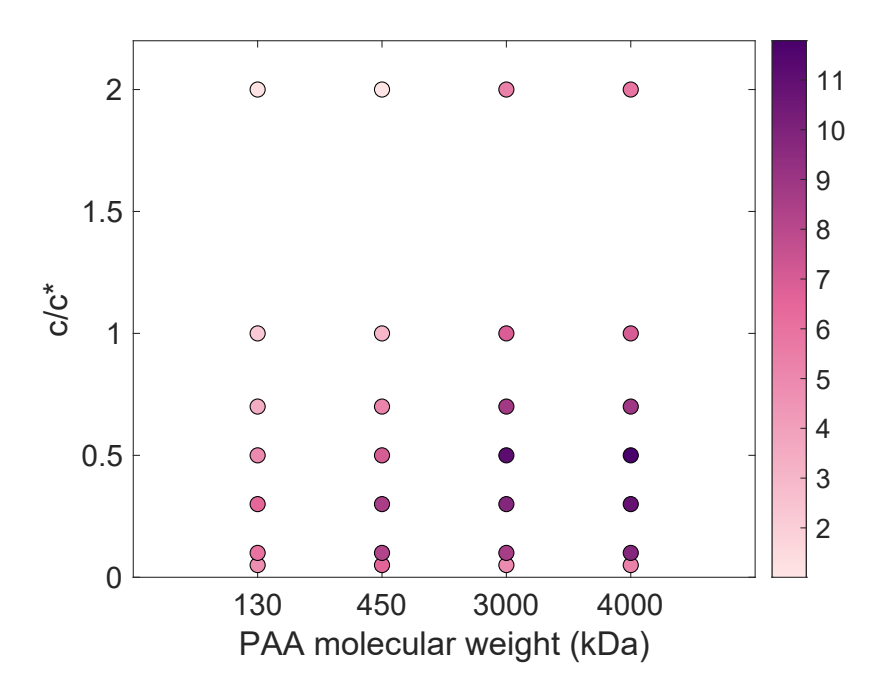


Figure 6: State diagram for bridging suspensions as a function of the PAA molecular weight and concentration. Points are colored by the value of the NDF (determined for a given molecular weight at the length scale maximizing the NDF for the suspension with largest clusters or strongest gel), as indicated by the color bar.

Conclusion

We show that polymer molecular weight $M_{\rm w}$ markedly alters the structure and dynamics of a bridging system consisting of TtMA copolymer particles and adsorbing PAA of molecular weights 130, 450, 3000, and 4000 kDa. Suspensions containing 130 kDa PAA remain fluid-like across the range of normalized polymer concentrations investigated ($c/c^* = 0.05$ to 2) and exhibit local maxima in structural metrics (i.e., contact number and local structure) and slowest dynamics at a normalized concentration $c/c^* \approx 0.5$. The fluidization of these samples upon further increase in polymer concentration is due to steric stabilization of a growing fraction of the particles as the particle surfaces

become saturated with polymer. Suspensions containing 4000 kDa PAA exhibit arrested dynamics and larger clusters than at 130 kDa, with similar non-monotonic dependence of properties occurring at normalized concentrations $c/c^* > 0.7$. For both $M_{\rm w}$, the onset of non-monotonic behavior occurs at c/c^* values below those required for full steric stabilization of the particles, indicating that some particles become sterically stabilized even at modest c/c^* . Biphasic behavior, reflecting distinct populations of freely diffusing and flocculated arrested particles, is observed at $c/c^* = 0.5$ for both $M_{\rm w}$.

Our results confirm that the polymer $M_{\rm w}$ alters the size of flocs, as found in earlier studies, 21,23,25 and the microscopic dynamics. The methods employed here may prove useful to elucidate size effects of other types of bridging agents, such as microgel particles, 10,41 and other types of particles, such as emulsions, 20,42,43 on particle structure and dynamics. Further, the biphasic behavior occurring at selected $M_{\rm w}$ and c/c^* may offer an alternate route to obtaining favorable combinations of rheological properties for extrusion-based processes such as 3-D printing. 44 We anticipate that studies in this system of the bulk rheological properties will provide guidance towards formulating flowable, low-clogging particulate suspensions for these applications. Finally, we anticipate that similar studies in suspensions with variable particle size will enable a zoo of rheological behaviors, including shake gels, 45,46 rheopectic, 47,48 and thixotropic fluids, 49,50 to be connected to microscopic interactions.

Acknowledgement

The authors thank Professor Amanda Marciel for use of her dynamic light scattering machine (3-D LS Spectrometer (LS Instruments)). This work was supported by the National Science Foundation (Grant No. CBET-1803728) and the Welch Foundation (Grant No. E-1869).

Supporting Information Available

The Supporting Information contains confocal micrographs of all suspensions (Figure S1), structure

of 450 and 3000 kDa (Figure S2), dynamics of 450 and 3000 kDa (Figure S3), radius of gyration as a function of frames for 3000 kDa (Figure S4), particle trajectories and 3-D renderings of 450 and 3000 kDa (Figure S5), radial distribution function with error bars for all suspensions (Figure S6), mean squared displacements with error bars for all suspensions (Figure S7), MSDs as a function of a rescaled time to account for changes in background viscosity (Figure S8), shifted g(r) graphs for clarity (Figure S9), critical polymer concentration for surface saturation (Figure S10), state diagrams as a function of $R_g^p/R_{particle}$ (a) and maximum CN (b) (Figure S11), Yukawa potential of TtMA particles (Figure S12), and available binding sites for all PAA molecular weights and c/c^* (Table S1).

References

- (1) Dickinson, E. Food Polymers, Gels, and Colloids, 1st ed.; Woodhead Publishing, 1991.
- (2) Wei, M.; Zhang, F.; Wang, W.; Alexandridis, P.; Zhou, C.; Wu, G. 3D direct writing fabrication of electrodes for electrochemical storage devices. *J. Power Sources* **2017**, *354*, 134–147.
- (3) Areir, M.; Xu, Y.; Harrison, D.; Fyson, J. 3D printing of highlyflexible supercapacitor designed for wearable energy storage. *Mater. Sci. Eng. B* **2017**, 226, 29–38.
- (4) Kreuter, J. Colloidal Drug Delivery Systems, 1st ed.; CRC Press, 2019.
- (5) Poon, W. C. K. The physics of a model colloid–polymer mixture. *J. Phys. Condens. Matter* **2002**, *14*, R859.
- (6) Tuinier, R.; Fan, T.-H.; Taniguchi, T. Depletion and the dynamics in colloid–polymer mixtures. *Curr. Opin. Colloid Interface Sci.* **2015**, *20*, 66–70.
- (7) Huang, H.; Ruckenstein, E. The Bridging Force between Colloidal Particles in a Polyelectrolyte Solution. *Langmuir* **2012**, *28*, 16300–16305.

- (8) Lafuma, F.; Wong, K.; Cabane, B. Bridging of colloidal particles through adsorbed polymers. *J. Colloid Interface Sci.* **1991**, *143*, 9–21.
- (9) Chen, J.; Kline, S. R.; Liu, Y. From the depletion attraction to the bridging attraction: the effect of solvent molecules on the effective colloidal interactions. *J. Chem. Phys.* **2015**, *142*, 084904.
- (10) Zhao, C.; Yuan, G.; Jia, D.; Han, C. C. Macrogel induced by microgel: bridging and depletion mechanisms. *Soft Matter* **2012**, *8*, 7036.
- (11) Smellie, R. H., Jr; La Mer, V. K. Flocculation, subsidence and filtration of phosphate slimes.
 VI. A quantitative theory of filtration of flocculated suspensions. J. Colloid Interface Sci.
 1958, 13, 589.
- (12) Alam, N.; Hampton, M. A.; Nguyen, A. V. Dewatering of coal plant tailings: Flocculation followed by filtration. *Fuel* **2011**, *90*, 26–35.
- (13) Vidgren, V.; Londesborough, J. 125th Anniversary Review: Yeast Flocculation and Sedimentation in Brewing. *J. Inst. Brew.* **2011**, *117*, 475–487.
- (14) Powell, C. D.; Quain, D. E.; Smart, K. A. The impact of brewing yeast cell age on fermentation performance, attenuation and flocculation. *FEMS Yeast Res.* **2003**, *3*, 149–157.
- (15) Wee, E. J. H.; Ngo, T. H.; Trau, M. A simple bridging flocculation assay for rapid, sensitive and stringent detection of gene specific DNA methylation. *Sci. Rep.* **2015**, *5*, 15028.
- (16) Sharma, K.; Sharma, M.; Modi, M.; Goyal, M.; Sharma, A.; Ray, P. Magnetic bead flocculation test: Improving the diagnosis of tuberculous meningitis (TBM) in low-resource settings. *Mol. Cell. Probes* 2020, *53*, 101595.
- (17) Anyfantakis, M.; Bourlinos, A.; Vlassopoulos, D.; Fytas, G.; Giannelis, E.; Kumar, S. K. Solvent-mediated pathways to gelation and phase separation in suspensions of grafted nanoparticles. *Soft Matter* **2009**, *5*, 4256–4265.

- (18) Zhang, C.; Yang, S.; Padmanabhan, V.; Akcora, P. Solution Rheology of Poly(acrylic acid)-Grafted Silica Nanoparticles. *Macromolecules* **2019**, *52*, 9594–9603.
- (19) Dickinson, E. Structure, stability and rheology of flocculated emulsions. *Current Opinion in Colloid and Interface Science* **1998**, *3*, 633–638.
- (20) Keane, D. P.; Mellor, M. D.; Poling-Skutvik, R. Responsive Telechelic Block Copolymers for Enhancing the Elasticity of Nanoemulsions. *ACS Applied Nano Materials* **2022**, *5*, 5934–5943.
- (21) Avadiar, L.; Leong, Y.-K.; Fourie, A. Effects of polyethylenimine dosages and molecular weights on flocculation, rheology and consolidation behaviors of kaolin slurries. *Powder Technol.* **2014**, 364–372.
- (22) Zhu, Z.; Li, T.; Lu, J.; Wang, D.; Yao, C. Characterization of kaolin flocs formed by polyacry-lamide as flocculation aids. *Int. J. Miner. Process.* **2009**, *91*, 94–99.
- (23) Schwarz, S.; Bratskaya, S.; Jaeger, W.; Paulke, B.-R. Effect of charge density, molecular weight, and hydrophobicity on polycations adsorption and flocculation of polystyrene latices and silica. *J. Appl. Polym. Sci.* **2006**, *101*, 3422–3429.
- (24) Ong, B. C.; Leong, Y. K.; Chen, S. B. Interparticle forces in spherical monodispersed silica dispersions: Effects of branched polyethylenimine and molecular weight. *J. Colloid Interface Sci.* **2009**, *337*, 24–31.
- (25) Otsubo, Y. Size effects on the shear-thickening behavior of suspensions flocculated by polymer bridging. *J. Rheol.* **1993**, *37*, 799–809.
- (26) Govedarica, A.; Bacca, E. J.; Trifkovic, M. Structural investigation of tailings flocculation and consolidation via quantitative 3D dual fluorescence/reflectance confocal microscopy. *J. Colloid Interface Sci.* **2020**, *571*, 194–204.

- (27) Pickrahn, K.; Rajaram, B.; Mohraz, A. Relationship between Microstructure, Dynamics, and Rheology in Polymer-Bridging Colloidal Gels. *Langmuir* **2010**, *26*, 2392–2400.
- (28) Kodger, T. E.; Guerra, R. E.; Sprakel, J. Precise colloids with tunable interactions for confocal microscopy. *Sci. Rep.* **2015**, *5*, 1436.
- (29) Park, N.; Umanzor, E. J.; Conrad, J. C. Aqueous Colloid + Polymer Depletion System for Confocal Microscopy and Rheology. *Front. Phys.* **2018**, *6*, 42.
- (30) Gallegos, M. J.; Soetrisno, D. D.; Park, N.; Conrad, J. C. Aggregation and gelation in a tunable aqueous colloid-polymer bridging system. *J. Chem. Phys.* **2022**, *11*, 114903.
- (31) Perruchot, C.; Khan, M. A.; Kamitsi, A.; Armes, S. P.; von Werne, T.; Patten, T. E. Synthesis of Well-Defined, Polymer-Grafted Silica Particles by Aqueous ATRP. *Langmuir* **2001**, *17*, 4479–4481.
- (32) Crocker, J. C.; Grier, D. G. Methods of Digital Video Microscopy for Colloidal Studies. *J. Colloid Interface Sci.* **1996**, *179*, 298–310.
- (33) Blair, D.; Dufresne, E. The Matlab Particle Tracking Code Repository. http://physics.georgetown.edu/matlab/.
- (34) Wang, Y.; Morawetz, H. Fluorescence Study of the Complexation of Poly(acrylic acid) with Poly(N,N-dimethylacrylamide-co-acrylamide). *Macromolecules* **1989**, 22, 164–167.
- (35) Pradip,; Maltesh, C.; Somasundaran, P.; Kulkarni, R. A.; Gundiah, S. Polymer-polymer complexation in dilute aqueous solutions: poly(acrylic acid)-poly(ethylene oxide) and poly(acrylic acid)-poly(vinylpyrrolidone). *Langmuir* **1991**, *7*, 2108–2111.
- (36) Broseta, D.; Leibler, L.; Strazielle, C. Universal Properties of Semi-Dilute Polymer Solutions: A Comparison between Experiments and Theory. *Europhys. Lett.* **1986**, *2*, 733.
- (37) Dibble, C. L.; Kogan, M.; Solomon, M. J. Structure and dynamics of colloidal depletion gels: Coincidence of transitions and heterogeneity. *Phys. Rev. Lett. E.* **2006**, *74*, 041403.

- (38) Hiemenz, P. C.; Rajagopalan, R. Principles of Colloid and Surface Chemistry.
- (39) Biggs, S. Steric and Bridging Forces between Surfaces Bearing Adsorbed Polymer: An Atomic Force Microscopy Study. *Langmuir* **1995**, *11*, 156–162.
- (40) Colby, R. Structure and linear viscoelasticity of flexible polymer solutions: comparison of polyelectrolyte and neutral polymer solutions. *Rheol. Acta* **2010**, *49*, 425–442.
- (41) Zhao, C.; Huan, G.; Han, C. C. Bridging and caging in mixed suspensions of microsphere and adsorptive microgel. *Soft Matter* **2014**, *44*, 8905–8912.
- (42) Helgeson, M. E.; Moran, S. E.; An, H. Z.; Doyle, P. S. Mesoporous organohydrogels from thermogelling photocrosslinkable nanoemulsions. *Nature Materials* **2012**, *11*, 344—-352.
- (43) Hsiao, L. C.; Doyle, P. S. Celebrating Soft Matter's 10th Anniversary: Sequential phase transitions in thermoresponsive nanoemulsions. *Soft Matter* **2015**, *11*, 8426–8431.
- (44) Conrad, J. C.; Ferreira, S. R.; Yoshikawa, J.; Shepherd, R. F.; Ahn, B. Y.; Lewis, J. A. Designing colloidal suspensions for directed materials assembly. *Curr. Opin. Colloid Interface Sci.* **2011**, *16*, 71–79.
- (45) Mar Ramos-Tejada, M.; Luckham, P. F. Shaken but not stirred: The formation of reversible particle polymer gels under shear. *Colloids Surf. A: Physicochem. Eng. Asp.* **2015**, *471*, 164–169.
- (46) Collini, H.; Mohr, M.; Luckham, P.; Shan, J.; Russell, A. The effects of polymer concentration, shear rate and temperature on the gelation time of aqueous Silica-Poly(ethylene-oxide) "Shake-gels". *J. Colloid Interface Sci.* **2018**, *517*, 1–8.
- (47) Potanin, A. Thixotropy and rheopexy of aggregated dispersions with wetting polymer. *J. Rheol.* **2004**, *48*, 1279.

- (48) Duman, O.; Tunç, S.; Çetinkaya, A. Electrokinetic and rheological properties of kaolinite in poly(diallyldimethylammonium chloride), poly(sodium 4-styrene sulfonate) and poly(vinyl alcohol) solutions. *Colloids Surf. A: Physicochem. Eng. Asp.* **2012**, *394*, 23–32.
- (49) Pignon, F.; Magnin, A.; Piau, J.-M. Thixotropic behavior of clay dispersions: Combinations of scattering and rheometric techniques. *J. Rheol.* **1998**, *42*, 1349.
- (50) Ong, E.; O'Byrne, S.; Liow, J. L. Yield stress measurement of a thixotropic colloid. *Rheol. Acta.* **2019**, *58*, 383–401.

TOC Graphic

